LAWRENCE
LIVERMORE
NATIONAL
LABORATORY

LLNL-TR-664835

Recent Progress Validating the HADES Model of LLNL's HEAF MicroCT Measurements

W. T. White, K. P. C. Bond, K. P. Lennox, M. B. Aufderheide, I. M. Seetho, G. P. Roberson

December 1, 2014

Disclaimer

This document was prepared as an account of work sponsored by an agency of the United States government. Neither the United States government nor Lawrence Livermore National Security, LLC, nor any of their employees makes any warranty, expressed or implied, or assumes any legal liability or responsibility for the accuracy, completeness, or usefulness of any information, apparatus, product, or process disclosed, or represents that its use would not infringe privately owned rights. Reference herein to any specific commercial product, process, or service by trade name, trademark, manufacturer, or otherwise does not necessarily constitute or imply its endorsement, recommendation, or favoring by the United States government or Lawrence Livermore National Security, LLC. The views and opinions of authors expressed herein do not necessarily state or reflect those of the United States government or Lawrence Livermore National Security, LLC, and shall not be used for advertising or product endorsement purposes.

This work performed under the auspices of the U.S. Department of Energy by Lawrence Livermore National Laboratory under Contract DE-AC52-07NA27344.

Recent Progress Validating the HADES Model of LLNL's HEAF MicroCT Measurements

W. Travis White III, Karina P. C. Bond, Kristin P. Lennox,

Maurice B. Aufderheide, Isaac M. Seetho, G. Patrick Roberson

Lawrence Livermore National Laboratory

Livermore, CA 94551

1. Executive Summary

This report compares recent HADES calculations of x-ray linear attenuation coefficients to previous MicroCT measurements made at Lawrence Livermore National Laboratory's High Energy Applications Facility (HEAF). The chief objective is to investigate what impact recent changes in HADES modeling have on validation results. We find that these changes have no obvious effect on the overall accuracy of the model. Detailed comparisons between recent and previous results are presented.

2. Introduction

The Livermore Explosives Detection Program (LEDP) uses the computer code HADES [Aufderheide 2000, 2004, 2013] to model measurements of x-ray linear attenuation coefficients (LAC) of explosives measured with the MicroCT system in Lawrence Livermore National Laboratory's (LLNL's) High Explosives Application Facility (HEAF). Goals of the modeling include estimating trends in LAC values as functions of composition, density and diameter; providing approximate expected values against which to compare measurements; and, potentially, replacing measurements with simulations. To meet these goals with confidence it is necessary to understand how well HADES calculations match measured results. Because the HADES models for the HEAF MicroCT system are refined from time to time as new information is acquired or the system is modified, the process of validating the model against MicroCT measurements is an ongoing task.

This paper compares recent HADES calculations of the linear attenuation coefficients μ_H and μ_L to previous measurements on the HEAF MicroCT system and to similar validation work by others, who have used the same experimental data as used here [Chen 2011, Lennox 2011, 2014(1) and 2014(2)]. The subscripts H and L refer to "high" and "low" energy beams from the MicroCT x-ray tube — 160kV bias voltage and 100kV bias voltage, respectively. The measured LACs come from reconstructed images of computerized tomographic (CT) x-ray scans and from analyses of individual digital radiographs (DR) obtained during those scans.

The main objective of the report is to investigate the impact that three changes have on validation results. First, we use a recently recalculated HADES baseline spectrum obtained by Aufderheide *et al.* [Aufderheide 2013], who updated the construction details of both the MicroCT x-ray tube and the detector array. Next, we add a 1.6359mm-thick *ad hoc* aluminum filter to the HADES beam path in order to produce statistically unbiased estimates of LAC. Finally, we compensate the experimental data for a drop-off

LLNL-TR-664835

of MicroCT output that occurred over the five months in which measurements were taken.

The report is organized into seven more sections. Section 3 provides background information. Section 4 discusses MicroCT measurements of LAC. Section 5 describes single-ray-path models for estimating LAC values. Section 6 discusses optimizing the HADES spectral model of the HEAF MicroCT System. Section 7 presents results. Section 8 summarizes. Section 9 suggests future work. Several appendices provide additional supporting details.

3. Background

3.1 HEAF MicroCT System

The HEAF MicroCT system has several components. A two-tray carousel holds a single cylindrical test specimen on its upper tray and six cylindrical reference specimens for quality assurance (QA) purposes on its lower tray. A bremsstrahlung x-ray tube with a sub-mm width spot simultaneously illuminates both trays of the carousel through a two-slit tungsten collimator, and an amorphous silicon x-ray panel detector records the digital radiographs. The cylindrical axes of the specimens are parallel to the axis of rotation of the carousel and perpendicular to the collimated fan beam passing through the main specimen on the top shelf of the carousel. Each MicroCT scan uses 400 angular views in steps of ½° at a given source voltage and detector integration time. Two x-ray voltages are used, 100kV with an aluminum sheet-metal x-ray filter and 160kV with the same aluminum filter plus an additional copper filter. The experimental setup is described elsewhere in more detail [Smith 2011, Chen 2011, Lennox 2012 – 2014] and will not be described further here.

3.2 HADES

HADES is a radiographic simulation computer code developed and used by LLNL for a variety of applications. [Aufderheide 2000 and 2004] It uses ray-tracing techniques coupled to a library of atomic spectral properties [Cullen 1989] to model transmission radiography. A link to the CAD modeling software BRL-CAD [Butler 2002] enables detailed geometric modeling of objects and the components of the x-ray system. HADES can operate in batch mode, making it useful for doing parameter studies such as calculating the LAC of hundreds of materials in a single run. The set of all user-provided input together with the HADES code itself and BRL-CAD constitutes a HADES model of a system. Appendix D describes the software structure of HADES models used in this report.

The HADES model of the HEAF MicroCT system has grown from a simplified, one-spatial-dimension approximation to a full-scale radiographic simulator capable of making both individual radiographs and collections of radiographs (scans) like those used in computerized tomography (CT). Currently, one key step remains in generating complete full-frame, end-to-end simulations of HEAF MicroCT system CT measurements: to apply image reconstruction software to HADES simulated scans, analyzing the results in the same way that experimental CT scans are analyzed. Such an end-to-end, complete simulation capability is planned for the future. At present, however, all HADES

simulations used to date by LEDP model the LAC by tracing rays along a single, judiciously chosen ray path.

3.3 Previous Validation Efforts

Chen *et al.* [Chen 2011] published the first report on validating the HADES model of the HEAF MicroCT against measured radiographs. In that report, the chief metric for validation was the LAC of a central ray through a cylindrical specimen when the specimen was centered on the main x-ray axis of the HEAF MicroCT system. Chen *et al*. compared against measurements of 18 specimens chosen from 7 materials, each measured with 4 spectra. They reported a mean absolute-value of error of 2.4%, with relative errors spanning the ranges [–5.4%, 5.4%] at 100kV and [–1.7%, 7.2%] at 160kV.

Lennox *et al*. [Lennox 2014(1)] performed similar comparisons using most of the same experimental data as Chen but with a slightly different method to estimate absorbance from experimental radiographs. They obtained a spread of relative errors similar to Chen's: [-2.9%, 5.4%] at 100kV and [0.0%, 6.9%] at 160kV. In addition, Lennox *et al*. [Lennox 2012] spent considerable effort trying to determine the accuracy of the experimental data by using the measurements of the HEAF MicroCT reference specimens as an indicator of experimental variability. They concluded that the worst-case upper bound on the relative error of HADES was about 7.8% at 100kV and about 9.6% at 160kV for the materials examined and that HADES predictions generally lay within the estimated bounds of experimental accuracy for each primary (*i.e.*, not reference) specimen.

Lennox *et al*. [Lennox 2014(1)] also compared HADES simulations of an entire MicroCT scan of the six reference specimens to measured radiographs and found generally good agreement between measurements and simulations, although the simulation appeared to suffer from a slight error in magnification. Additionally, in a recent report, they [Lennox 2014(2)] compared single-ray HADES estimates of LAC values to those obtained from reconstructed CT images measured with the HEAF MicroCT. As a result of the latter study, Lennox *et al.* concluded that using experimental beam-hardening compensation (BHC) coefficients provided better agreement between model and CT measurements than using HADES-derived BHC coefficients. Even with the improved agreement, however, modeling errors for the CT-derived values were significantly larger than errors which used individual single-ray estimates from DR images.

Aufderheide *et al*. [Aufderheide 2013] considered the peak absorbance of a set of three materials (graphite, polytetrafluoroethylene [PTFE], and silicon) and, after adding an *ad hoc* 3.3mm-thick aluminum spectral filter to the model, produced HADES calculations that lay within 4% of measured values at 100kV and 160kV. Such close agreement is within the uncertainty of the x-ray attenuation cross sections used in HADES [Cullen 1989, Aufderheide 2007]. Prior to adding the aluminum filter, Aufderheide updated the baseline HADES spectral models for the HEAF panel detector and source, refining construction details and recalculating the detector and source properties by using MCNP 5 [Briesmeister 2000]. The calculations in the present work use that updated baseline spectral model.

4. HEAF MicroCT Measurements of LAC Values

The measured data in this paper come from scans taken between January and May in 2010 as part of LEDP's Test Plan 35 (TP35). [Krauss 2009] Fourteen cylindrical solids of homogeneous, well known composition, density and diameter are used as experimental test specimens (Table 1). They are a subset of the specimens first reported by Chen *et al*. and subsequently by Lennox *et al*. [Chen 2011, Lennox 2011–2014] Four of the specimens used previously are not considered here, because those measurements are suspect (see Appendix A). In the remainder of this paper, when we compare measurements to HADES calculations, previous or present, we are referring only to the fourteen measurements listed in Table 1.

Table 1. *Measurements used in this work listed in order of increasing effective atomic number, Ze.* [Chen 2011]

Name	Diameter (cm)	Density (gm/cm^3)	Effective Atomic Number, Ze	Date (yy-mm-dd)
Graphite, half inch	1.302	1.817	6	10-04-01
Graphite , one inch	2.501	1.658	6	10-04-13
Graphite, two inches	5.015	1.737	6	10-03-29
Acetyl Copolymer, half inch	1.267	1.412	7	10-04-07
Acetyl Copolymer, one inch	2.548	1.41	7	10-05-07
Acetyl Copolymer, two inches	5.090	1.396	7	10-05-12
Water, one inch	2.715	0.998	7.42	10-01-27
Water, two inches	4.770	0.998	7.42	10-03-30
PTFE, one inch	2.565	2.151	8.43	10-01-06
PTFE, two inches	5.528	2.171	8.43	10-04-12
Magnesium, half inch	1.288	1.745	12	10-04-06
Silicon, half inch	1.264	2.323	14	10-05-14
Silicon, one inch	2.535	2.324	14	10-05-18
Titanium, half inch	1.289	4.49	22	10-04-09

None of the x-ray scans of any specimen in Table 1 is repeated. Therefore, it is difficult to get a direct estimate of the variability of the results of individual test specimens at a given x-ray voltage. Lennox *et al.* [Lennox 2014(1)] strongly recommend scanning each specimen multiple times at each source voltage in order to understand measurement uncertainty better and to estimate useful statistical confidence intervals.

The MicroCT system is known to have changed through-out the months in which the x-ray scans of Table 1 were obtained, as evidenced by a drop in estimated LAC values of the six lower-tray reference specimens. For example, the change in μ_H is of the order of 2–3% in the aluminum reference specimen. (See Figure 2 in [Lennox 2014(2)].) To compensate for the system change Lennox calculates a correction for the data by using a piecewise linear fit that is constant before early March 2010 and follows a declining linear trend afterwards. [Lennox 2014(3)] We apply those proposed corrections in this work.

The correction proposed by Lennox is based on LAC values from reconstructed CT images. It is given by the following:

$$(\mu_{\mathrm{L}})_{\mathrm{Corrected}} = \begin{cases} \mu_{\mathrm{L}}, \text{Before 3 March 2010 and between 9-22 April 2010, inclusive} \\ \dfrac{\mu_{\mathrm{L}}}{1-0.000465d}, \text{After 3 March 2010, } d = \text{days past 3 March 2010} \end{cases} \tag{1a}$$

$$(\mu_{\mathrm{H}})_{\mathrm{Corrected}} = \begin{cases} \mu_{\mathrm{H}}, \text{On or before 1 March 2010} \\ \dfrac{\mu_{\mathrm{H}}}{1-0.000196d}, \text{After 1 March 2010, } d = \text{days past 1 March 2010} \end{cases} \tag{1b}$$

4.1 Estimating μ from Individual Digital Radiographs (DR)

In this report, as in previous works [Chen *et al.* 2011, Lennox *et al.* 2014(1)], we use the peak absorbance measured from a single DR image to estimate the LAC through the center of a cylinder. By *absorbance* we mean $\ln(I_o/I)$, where I_o is the (incident) irradiance of the beam when the object is not in the beam and I is the (transmitted) irradiance when the object is in the beam. Figure 1 illustrates the variation of absorbance across a cylinder as determined from a HEAF MicroCT attenuation radiograph, an image in which every pixel value is the local absorbance of a narrow ray bundle.

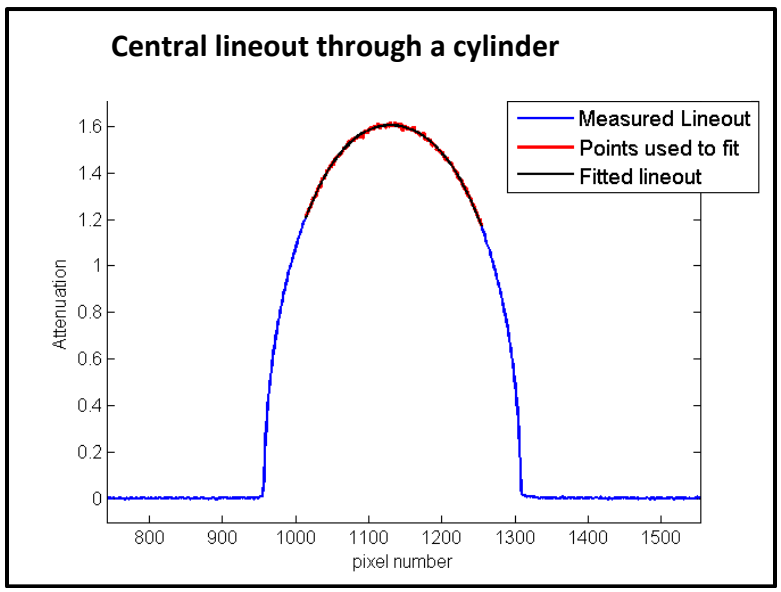

Figure 1. *Lineout along the horizontal centerline of the top slit in the attenuation radiograph (blue). The red indicates the section of the data that was used to fit a polynomial, and the black line is the fitted data.*

Along any given ray path, the absorbance and the effective linear attenuation coefficient of the material, μ, are related by

$$\mu = \frac{1}{L}\ln\left(\frac{I_o}{I}\right). \tag{2}$$

In Eq(2), L is the x-ray path length through the specimen [*e.g.*, de Jonge 2004].

Figure 2 below shows a 2-slit MicroCT radiograph from a typical scan, with the various key features labeled. To estimate μ directly from a single radiograph from a CT scan set,

we first find the radiograph from a given scan set such that the test specimen is centered on the central axis of the x-ray system and is closest to the x-ray source, as described in Appendix C. Once the radiograph of interest has been identified, we make a "reciprocal-transmittance" radiograph of I_o/I along the central five rows of the upper slit. To account for intensity changes during a scan, we monitor the mean signal in an unobscured 7x100 rectangular patch of pixels, the "Postage Stamp" region (shown as a green rectangle in Figure 2) and scale the entire radiograph by multiplying it by the ratio $I^{(PS)}/I_o^{(PS)}$. The latter expression is the ratio of mean signals in the postage stamp region. We then calculate the absorbance everywhere in the five-rows-high image and create an attenuation radiograph.

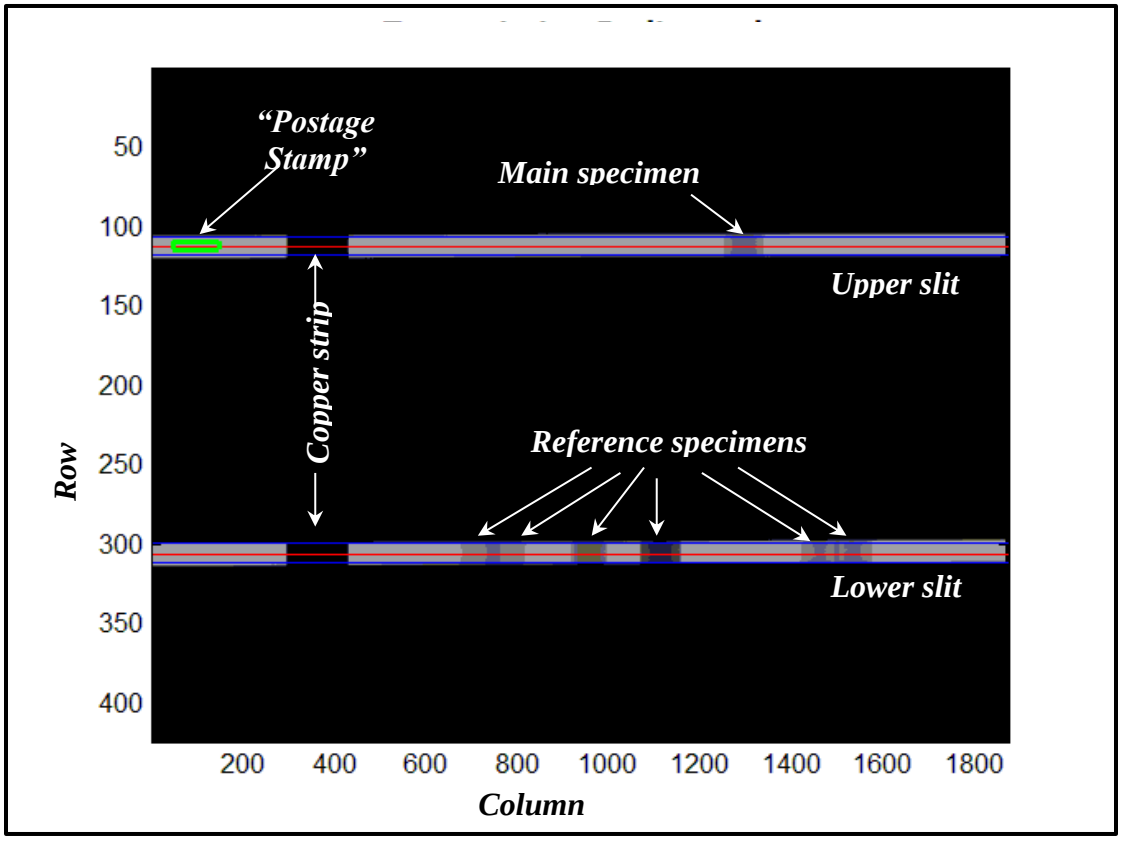

Figure 2. *MicroCT radiograph.* The red lines are the center lines of the slits as identified by our data processing. The green box represents the location and size of the "postage stamp" region.

Next we next find the median value column-wise across central portion of the five-row-high image of the upper slit. Doing so yields a single lineout as in Figure 1 (blue line). The absorbance is zero to the side of the specimen, rises smoothly across the specimen to a maximum and then falls smoothly back to zero on the other side of the specimen, apart from noise. To estimate the peak absorbance from the data, we fit a fourth-degree polynomial to the central section of the lineout through the specimen (about 1/3 the width of the specimen) and use the peak value of the fitted function as a best estimate of μL. Dividing this value by $L = D$ yields the measured value of μ along a diameter. We then scale the result of Eq(2) according to Eq(1a) or (1b), to compensate for drift of the HEAF MicroCT system and save the result for comparison to a HADES calculation.

4.2 Estimating μ from CT Reconstructed Images

Estimating μ from a reconstructed CT image is a different process than estimating it from a DR image. First, unlike the DR images, the reconstructed images used by LEDP are compensated for beam hardening, discussed below. Second, a reconstructed CT image is a 3-D image in which the value stored in each volume element (*voxel*) is a direct estimate of μ, not an absorbance value, as in an attenuation radiograph. Therefore, in a CT image, one must average μ over all voxels of interest to estimate the LAC value of a specimen. In this section, we discuss the Beam-Hardening Compensation (BHC) and averaging methods used to process the experimental CT data in this report. The section concludes with mentioning a known bug that occurred in about half of the CT reconstructions. The error is completely repaired in our analyses.

Beam-Hardening Compensation (BHC)

For monoenergetic x-ray beams, μ in Eq(2) is independent of the distance L and, equivalently, of the thickness of the test specimen. However, for polyenergetic beams, μ declines as the path length L increases. This is because in every material x-rays at some energies are attenuated more than x-rays of other energies, and the more strongly attenuated x-rays are preferentially filtered out of the beam by the test object. For the test objects and x-ray energies of interest to LEDP, it is the low-energy x-rays that are preferentially filtered out of the beam as it propagates through a specimen. The mean x-ray energy of the transmitted beam therefore shifts to higher values ("harder" x-rays), and the mean LAC drops. This process is called "beam hardening."

To mitigate the effects of beam hardening on reconstructed CT images, the HEAF MicroCT reconstruction code, IMGREC [Bond 2014], applies a beam-hardening compensation (BHC) algorithm to CT measurements of μ [Schneberk 2010]. In the algorithm, the attenuation, $\mu \cdot L$, of each pixel in each attenuation radiograph of a scan is multiplied by the function $f_{BHC}(\mu \cdot L)$, where

$$f_{BHC}(\mu \cdot L) = \begin{cases} (0.814 + 0.2\mu \cdot L), & \text{for } \mu_L \\ 1, & \text{for } \mu_H \end{cases} \quad \text{[LLNL's aluminum-based BHC function].} \quad (3)$$

After the BHC algorithm has been applied, the image is then reconstructed.

The intent of BHC is to convert the measured absorbance to a value that is the thin-specimen value of μ for the test specimen, regardless of the thickness of the specimen. When the absorbance of a material is much less than unity, the value of μ approaches a thin-specimen limit. The thin-specimen limit of μ is a constant that is characteristic of the material of the test object and the x-ray spectrum of the incident beam, but it does not depend upon specimen thickness.

Ideally, a BHC algorithm works accurately with any material. In practice, BHC algorithms are based on a small number of reference materials and are rigorously accurate for only those materials. In 2010, the reference material used for the BHC algorithm during CT image reconstruction was aluminum. Such an algorithm tends to try to make the estimated value of the LAC to appear like that of aluminum. Consequently, it overcompensates for beam hardening in materials consisting only of elements of lower

atomic number than aluminum — elements such as hydrogen, carbon, nitrogen, oxygen and fluorine. The BHC algorithm introduces a systematic bias to the estimated LAC values for those materials.

Mean LAC from a CT Reconstruction

Following SOPs for MicroCT image reconstruction [DeMicco 2012] and data analysis, [Seetho 2011, Kallman 2012] the mean LAC values μ_H and μ_L are estimated for each specimen from the reconstructed CT images with beam hardening compensation applied as in Eq(3). The essence of the algorithm is first to isolate a disk of the cylindrical specimen that is seven slices thick and centered in the upper slit of the MicroCT system, second to erode the outer layers of the disk in order to reduce partial-volume artifacts, and third to take the arithmetic mean of the remaining voxels in the core of the disk.

Repair of a Known Bug

Two almost identical versions of IMGREC were used to reconstruct the CT images in this and previous works. A known bug in one of the two versions underestimates μ_H and μ_L (cm^{-1}) in some of the data by exactly 10% [Schneberk 2009]. This error is easy to fix by dividing the reconstructed values of a given scan by 0.9 when necessary, which we have done. Table 2 shows which reconstructed images required re-scaling, as indicated by a 0.9 in the columns for μ_L and μ_H, and those that do not, as indicated by a 1. After repairing the IMGREC bug and compensating for beam hardening, we correct μ_H and μ_L for system drift by applying Eqs(1a) and (1b). We then save the results for comparison to HADES. Appendix B provides a slightly more detailed description of the steps we have used to extract μ_H and μ_L from CT reconstructions.

Table 2. *Reconstructed images requiring correction in some versions of IMGREC (indicated by a "0.9" under the μ_H and μ_L columns).* Note: one specimen, Acetyl Copolymer One Inch, was reconstructed correctly for μ_H but not μ_L.

Specimen	μ_L	μ_H
Graphite, half inch	0.9	0.9
Graphite , one inch	0.9	0.9
Graphite, two inches	0.9	0.9
Acetyl Copolymer, half inch	0.9	0.9
Acetyl Copolymer, one inch	0.9	1
Acetyl Copolymer, two inches	1	1
Water, one inch	1	1
Water, two inches	1	1
PTFE, one inch	1	1
PTFE, two inches	1	1
Magnesium, half inch	0.9	0.9
Silicon, half inch	0.9	0.9
Silicon, one inch	1	1
Titanium, half inch	1	1

5. Single-Ray-Path Models of μ

This section describes two ways of using calculations along a single ray path either to simulate a measured LAC at a point in a DR or to simulate the mean LAC from a reconstructed CT image. Due to volumetric averaging and BHC used in the CT image but

not in the individual DR image, these two ways of determining LAC for a given specimen generally yield different values of μ. So do their simulations.

Conceptually, in the single-ray-path model, one calculates a 1-pixel transmission radiograph of I/I_o along a known path length L of material and then determines μ from Eq(2). In the calculation, the composition and density of the specimen and the spectral properties of the source, detector and object must be known, but details of the geometry are ignored, other than path length L. No collimator is included in the model, and detector blur is ignored. Geometrically, the model is equivalent to simulating an infinitely wide, uniformly intense, collimated beam passing through an infinitely wide slab of material and striking an infinitely wide planar detector array. Reducing the calculations to a single-pixel radiograph causes such simulations to be fast, and the technique has been applied for studying trends in LAC over changes in composition, density and thickness for large numbers of materials. The initial HADES validation papers for the MicroCT use this model. [Chen 2011, Lennox 2014(2)].

As the HADES model of the MicroCT system has progressed towards simulating full CT scans, the single-ray-path model has evolved. Instead of computing a 1-pixel radiograph of a planar slab specimen, one now computes an entire simulated attenuation radiograph of a cylinder using the full detector width. One then selects a single pixel of interest from the radiograph and saves only its simulated output. The rest of the radiograph is discarded. This "full-radiograph" approach includes effects of collimator slits and detector blur of neighboring pixels, whereas the original "single-pixel" approach ignores blur and neighboring pixels. All details of the geometry of the MicroCT experiment are now modeled. In the model the cylinder is centered laterally on the main axis of the x-ray system as close to the source as possible. (By *main axis* we mean the line through the center of the x-ray spot source and perpendicular to the axis of rotation of the MicroCT carousel.) In the present single-ray-path model, the pixel centered on the x-ray axis is the pixel of interest. The ray path lies along a diameter of the cylindrical specimen. While simulating a full radiograph takes considerably longer than computing a 1-pixel radiograph, it is faster than simulating an entire CT scan and reconstructing the image.

5.1 Single-Ray-Path Model for an Individual Projection

The key differences between simulating attenuation of the central ray in a DR image and simulating the mean value of μ in a CT scan are the choice of path length to use and the implementation (or not) of BHC. In the DR images simulated in this work, beam hardening is not compensated and the x-ray path length through the cylinder is $L = D$, where D is the diameter of the cylinder. This matches the conditions in the experimental DR projections being simulated. Denoting the simulated LAC for the central ray through the cylinder as μ_{Proj} we have

$$\mu_{\text{Proj}} = \frac{1}{D} \ln\left(\frac{I_o}{I}\right)\Bigg|_{L=D} . \tag{4}$$

In Eq(4), the absorbance $\ln\left(\frac{I_o}{I}\right)$ is understood to be computed along a diameter.

5.2 Single-Ray-Path Model for the Mean Value of μ in a Reconstructed CT Image

We now consider using the single-ray-path model to estimate the mean value of the LAC of a cylindrical object as determined by analyzing a reconstructed CT image. Let μ_{CT} denote that value. Further, let $\overline{L}$ denote the mean distance that all rays in the CT scan travel through the cylinder, and let $\overline{\mu}$ denote the mean value of the LAC through the cylinder in the absence of beam-hardening compensation. As shown in Appendix E,

$$\begin{aligned}\overline{\mu} &\approx \mu(\overline{L}) \\ &= \frac{1}{\overline{L}} \ln\left(\frac{I_o}{I}\right)\Bigg|_{L=\overline{L}} .\end{aligned} \tag{5}$$

In the MicroCT experiment, the fan-beam is almost a parallel-ray geometry. Thus, the mean path length across a cylindrical test object is approximately the mean chord length across the circular cross section of the cylinder, which for a circle of diameter D is $\overline{L} = \pi D / 4$. We rewrite Eq(5) accordingly (Appendix E):

$$\overline{\mu} = \frac{4}{\pi D} \ln\left(\frac{I_o}{I}\right)\Bigg|_{L=\pi D/4} . \tag{5'}$$

We then apply the experimentally obtained BHC function, Eq(3), to estimate μ_{CT}:

$$\mu_{\mathrm{CT}} \approx \left(\overline{\mu}\right) f_{BHC}\left(\overline{\mu}\overline{L}\right). \tag{6}$$

It is possible to derive a BHC function similar to Eq(3) based only on HADES. As mentioned above, however, Lennox *et al.* [Lennox 2014(2)] have shown that using Eq(3), the experimental BHC, in Eq(6) has smaller errors than deriving a BHC function with HADES and using it instead. Therefore, the experimentally derived BHC function is used for all HADES results compared to experimental μ_L values.

6. Optimizing HADES' spectral model of the HEAF MicroCT System

The accuracy of HADES depends strongly on the accuracy of the spectral models used to represent the source and detector. As pointed out by Aufderheide [Aufderheide 2013] and others, accurate, detailed spectral data on the source and detector used by the HEAF MicroCT system are not readily available, because some of the information is tightly held by vendors and some simply is unknown. Consequently, even after carefully constructing physical descriptions of the MicroCT source and detector and then making reasonable estimates of values of their unknown parameters, one may have spectral errors in the source intensity or the detector response function or both.

From a modeling point of view, the spectral intensity $S(E)$ and the spectral detection efficiency $D(E)$ are used in HADES as a product, $S(E)D(E)$. Here, E denotes x-ray photon energy. To correct spectral errors in the model of the MicroCT system, it is sufficient to find a spectral function that corrects the product $S(E)D(E)$.

Aufderheide *et al*. [Aufderheide 2013] recently attempted to do this based on physical arguments. Conceivably, the MicroCT panel detector or source may have undocumented sheet(s) of material hidden to the eye that act as spectral filters. By inserting a sheet of a possible spacer or window material into the modeled beam and adjusting the thickness (areal density) of the material, one modifies the product $S(E)D(E)$. Without any additional material in the modeled beam — *i.e.*, using the best possible estimate of the spectrum of the MicroCT system — Aufderheide observed that the HADES model of μ for three materials (graphite 2in diameter, PTFE 2in diameter, and silicon 1in diameter) had a bias to their errors, and the maximum error between model and measurement was much larger than the limiting uncertainty in the modeled material properties of the specimens. For an unbiased model, the mean error should be zero. Aufderheide introduced a 3.3mm (~$^1/_8$ inch) thick aluminum filter into the modeled beam, representing for example a possible hidden sheet inside the HEAF MicroCT panel detector. As a result, the maximum difference between calculated and measured LAC dropped to less than 4% in absolute value. Such an error is of the order expected for the library of LAC values used by HADES. [Cullen 1989 and Aufderheide 2007]

We have applied Aufderheide's method using 14 test specimens instead of 3. Figure 3 shows a scatterplot of the resulting modeling errors for μ_L and μ_H. By *modeling error* we mean the relative difference between model and measurements, ε, expressed as a percentage.

$$\varepsilon \equiv (\mu_{\text{model}} - \mu_{\text{measurement}}) / (\mu_{\text{measurement}}). \tag{7}$$

As the figure shows, error values run from about -7% to +3.5%, a range of 10.5%, and the mean error is not zero. The spectrum used in the figure is the same spectrum used in [Aufderheide 2013], including a 3.3mm-thick *ad hoc* aluminum filter.

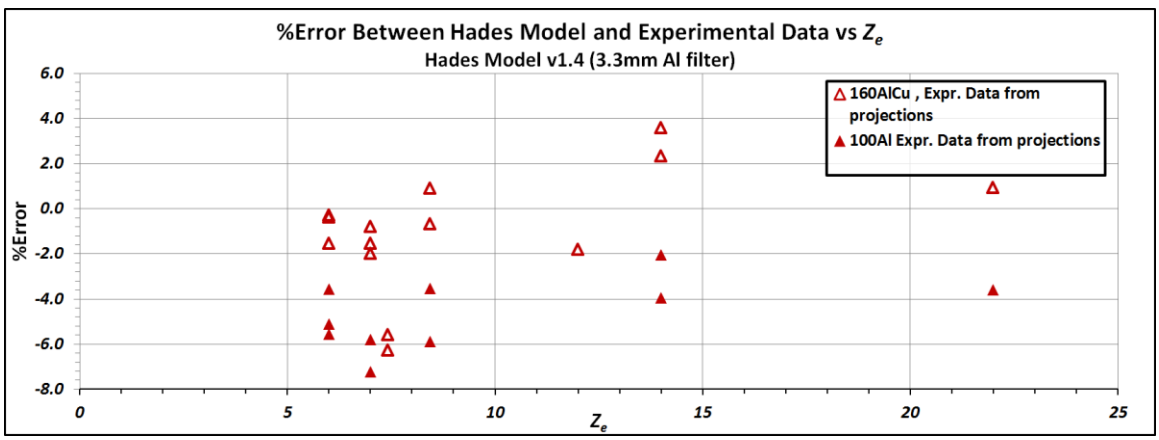

Figure 3. *Modeling error versus effective atomic number (Z_e) for the materials in Table 3 for 100Al (solid red triangles) and 100AlCu (hollow red triangles) with a 3.3mm aluminum plate. Error values run from about -7% to +3.5%, a range of 10.5%.*

In order to remove the statistical bias in the distribution of modeling errors, we have experimented with additional spectral adjustments. In doing so, we use only values of μ determined from individual radiographs, not from CT reconstructions. This is because individual measured radiographs provide a more direct assessment of HADES than the CT reconstructions. CT analyses suffer from numerical artifacts such as beam hardening

compensation, partial volume effects and angular under-sampling. Three optimization tests that we explored are listed below.

(a) Adjust the thickness of the *ad hoc* filter of aluminum to minimize the mean error. Introducing this aluminum gives an unbiased distribution of error values. As already stated, it represents the presence of a possible hidden sheet of material in either the detector or the source or both. We find that the optimal thickness of additional aluminum is 1.6359 mm (Figure 4), which is a plausible amount of material, given the uncertainties in construction of both the source tube and the detector panel. We have elected to use this modification to define the optimized spectrum. However, the improved results do not mean that a hitherto unknown 1.6359mm-thick sheet of aluminum is actually physically present in the MicroCT system.

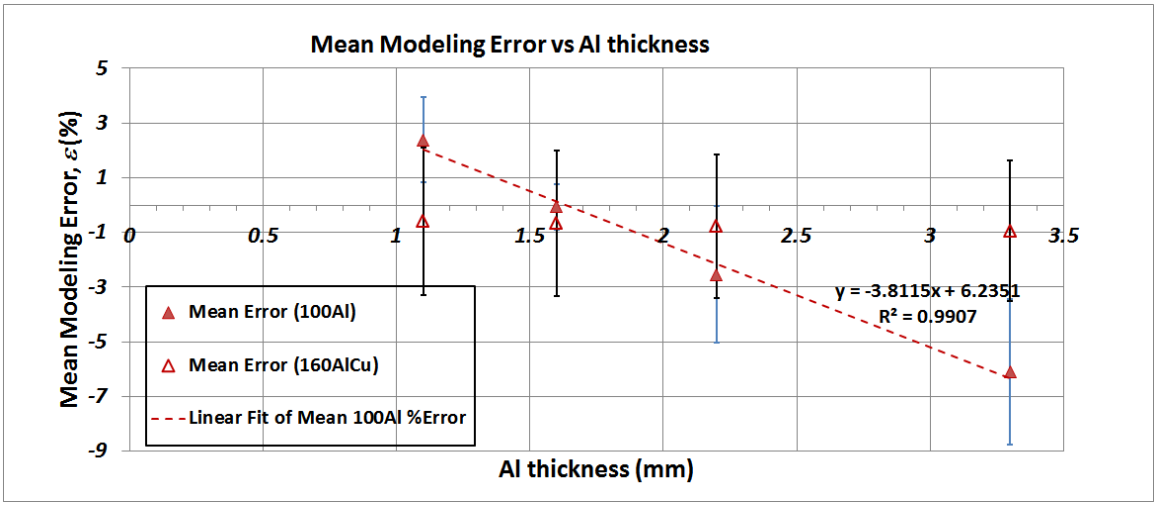

Figure 4. *Mean error over all 14 test materials as a function of thickness of the added Al filter.* Note that the mean error at 160kV is insensitive to the added Al filter. The mean error at 100kV is zero for a thickness of 1.6359mm.

(b) Add an *ad hoc* filter of tungsten (W) instead of Al, and adjust its thickness to minimize the mean error. This correction represents compensating for an error in the takeoff angle of x-rays emanating from the tungsten anode in the source, which would affect the internal beam hardening of the emitted beam. This method works satisfactorily, but the mean error at 100kV is highly nonlinear. The optimal thickness is about 13 μm (Figure 5).

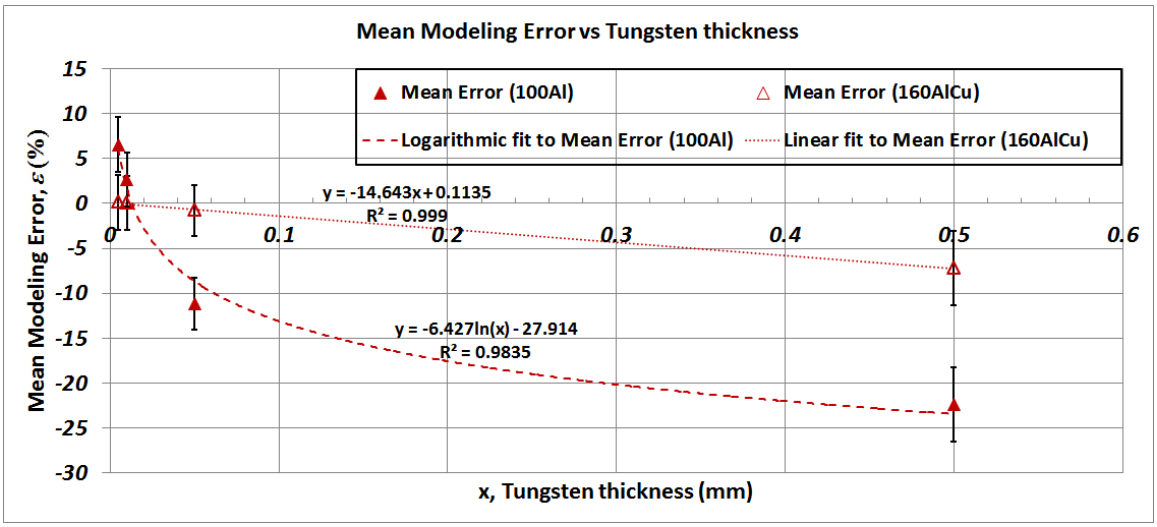

Figure 5. *Mean error over all 14 test materials as a function of thickness of the added tungsten filter.* The mean error at 100kV is zero for a thickness of 13 μm.

(c) Adjust the ratio of the line emissions to the broad-band (continuum) emissions in the source spectrum. This corresponds loosely to a variation in the depth of penetration of electrons into the anode in the source. This method requires an order of magnitude increase in the estimated line emissions at 100kV to minimize the mean error. The baseline spectrum is computed with MCNP 5 [Briesmeister 2000], a well-tested code, and such an increase is not believable. Therefore this approach is abandoned currently but may be investigated further in the future. Figure 6 shows the line and continuum features in the baseline x-ray source spectra used to model the HEAF MicroCT System.

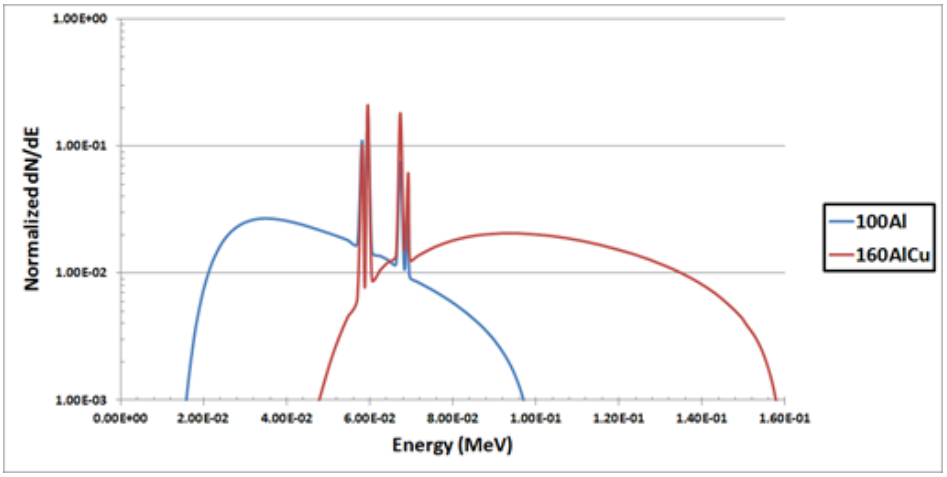

Figure 6. *Baseline x-ray source spectra at 100kV and 160kV showing the line emissions (spikes) and the underlying continuum emissions.*

We find that the main effect of modifying the spectrum — whether by adding an *ad hoc* metal filter or by adjusting the ratio of line strength to continuum — is to shift the mean error up and down. The overall range of modeling error values (Max-Min) changes only slightly, except when trying to optimize the ratio of power in the continuum to power in the line spectra.

7. Validation Results

Figure 7 and Tables 3 and 4 compare our single-ray-path HADES calculations to HEAF MicroCT measurements. The HADES spectrum is optimized with an *ad hoc* 1.6359mm-thick aluminum filter using only DR results. Figure 7 graphs modeling errors for μ_L and μ_H for both CT and DR data. As the figure shows, the errors for CT-derived values (diamonds) span a larger range, [-5%, 12%], than those for DR-derived values (triangles), [-6%, 5%]. Tables 3 (100kV) and 4 (160kV) display the same results on a specimen-by-specimen basis.

Table 5 (DR at 100kV), Table 6 (DR at 160kV) and Table 7 (CT at both 100kV and 160kV) compare our results to previous results [Chen 2011, Lennox 2014(1) and 2014(2)]. The mean absolute values and range of modeling errors among all three groups are comparable, indicating that the various methods used are not significantly different from each other. In Tables 5 through 7, all measured values have been compensated for the downward MicroCT trends after about March 1, 2010, using Eqs(1a) and (1b). This was not done in the original papers of Chen *et al.* and Lennox *et al.*, but it has been done here, which results in slight differences between the numbers below and those in the earlier works. It is not clear the correction improves the overall agreement with HADES.

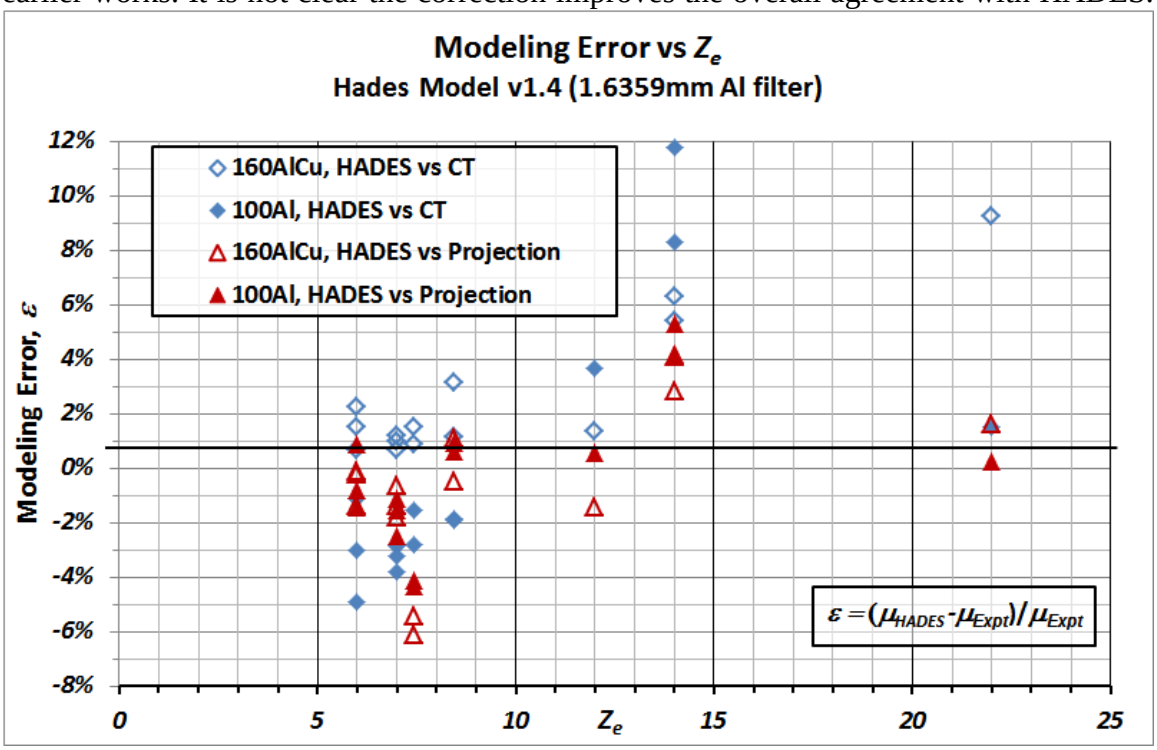

Figure 7. *Modeling error between the attenuation predicted by HADES central-axis method and that estimated from experimental CT reconstructions (blue) and from individual projections (red) for two energy channels, 100Al (solid markers) and 160AlCu (hollow markers) for fourteen materials.*(See Tables 3 and 4.)

Table 3. *Comparison of HADES calculations to HEAF MicroCT measurements at 100kV for μ_L in 14 test specimens.*

100 Al (μ_L)								
Material	Nominal Diameter (in.)	Dia. (cm)	Mean Attenuation (CT)			Central Ray (DR)		
			μ_{HADES_BHC} (cm^{-1})	μ_{CT_BHC} (cm^{-1})	ε	μ_{HADES} (cm^{-1})	μ_{Proj} (cm^{-1})	ε
Graphite	0.5	1.302	0.333	0.343	-3.0%	0.373	0.376	-0.8%
	1	2.501	0.322	0.325	-1.1%	0.338	0.335	0.9%
	2	5.015	0.381	0.401	-4.9%	0.347	0.352	-1.5%
Acetyl Copolymer	0.5	1.267	0.305	0.317	-3.8%	0.344	0.353	-2.5%
	1	2.548	0.322	0.332	-2.9%	0.337	0.342	-1.5%
	2	5.09	0.351	0.363	-3.2%	0.322	0.326	-1.1%
Water	1	2.715	0.247	0.250	-1.6%	0.263	0.275	-4.1%
	2	4.77	0.261	0.269	-2.8%	0.256	0.267	-4.3%
PTFE	1	2.565	0.550	0.560	-1.8%	0.523	0.520	0.6%
	2	5.528	0.623	0.635	-1.9%	0.486	0.481	0.9%
Magnesium	0.5	1.288	0.725	0.699	3.7%	0.721	0.717	0.6%
Silicon	0.5	1.264	1.247	1.116	11.8%	1.12	1.06	5.3%
	1	2.535	1.212	1.119	8.3%	0.941	0.903	4.2%
Titanium	0.5	1.289	4.871	4.799	1.5%	3.021	3.014	0.2%
				Min. ε	-4.9%		**Min. ε**	-4.3%
				Max. ε	11.8%		**Max. ε**	5.3%
				Mean $\lvert\varepsilon\rvert$	3.7%		**Mean $\lvert\varepsilon\rvert$**	2.0%

Table 4. *Comparison of HADES calculations to HEAF MicroCT measurements at 160kV for μ_H in 14 test specimens*

160 AlCu (μ_H)								
Material	Nominal Diameter (in.)	Dia. (cm)	Mean Attenuation (CT)			Central Ray (DR)		
			μ_{HADES} (cm^{-1})	μ_{CT} (cm^{-1})	ε	μ_{HADES} (cm^{-1})	μ_{Proj} (cm^{-1})	ε
Graphite	0.5	1.302	0.280	0.278	0.7%	0.280	0.284	-1.4%
	1	2.501	0.257	0.251	2.2%	0.2569	0.2573	-0.1%
	2	5.015	0.269	0.265	1.5%	0.269	0.270	-0.2%
Acetyl Copolymer	0.5	1.267	0.236	0.234	0.7%	0.236	0.241	-1.8%
	1	2.548	0.237	0.234	1.0%	0.237	0.240	-1.4%
	2	5.09	0.235	0.232	1.2%	0.235	0.236	-0.6%
Water	1	2.715	0.176	0.175	0.9%	0.177	0.188	-6.1%
	2	4.77	0.177	0.174	1.5%	0.177	0.187	-5.4%
PTFE	1	2.565	0.336	0.333	1.2%	0.337	0.338	-0.5%
	2	5.528	0.339	0.329	3.1%	0.338	0.335	1.1%
Magnesium	0.5	1.288	0.323	0.319	1.3%	0.324	0.328	-1.4%
Silicon	0.5	1.264	0.486	0.457	6.3%	0.485	0.466	4.1%
	1	2.535	0.481	0.457	5.4%	0.478	0.465	2.8%
Titanium	0.5	1.289	1.429	1.308	9.3%	1.383	1.361	1.6%
				Min. ε	0.7%		**Min. ε**	-6.1%
				Max. ε	9.3%		**Max. ε**	4.1%
				Mean $\lvert\varepsilon\rvert$	2.6%		**Mean $\lvert\varepsilon\rvert$**	2.0%

Table 5. *Comparison of values for individual projections reported in this work to previous similar work at 100kV.*

		100kV Central Ray (DR) Results								
		Chen *et al.*			Lennox *et al.*			This Paper		
Material	Nominal Diameter (in.)	μ_{HADES} (cm^{-1})	μ_{Proj} (cm^{-1})	ε	μ_{HADES} (cm^{-1})	μ_{Proj} (cm^{-1})	ε	μ_{HADES} (cm^{-1})	μ_{Proj} (cm^{-1})	ε
Graphite	0.5	0.37	0.37	-0.1%	0.369	0.369	0.0%	0.373	0.376	-0.8%
	1	0.33	0.33	0.0%	0.332	0.332	0.0%	0.338	0.335	0.9%
	2	0.34	0.35	-1.7%	0.343	0.349	-1.7%	0.347	0.352	-1.5%
Acetyl Copolymer	0.5	0.34	0.34	-1.2%	0.339	0.347	-2.3%	0.344	0.353	-2.5%
	1	0.33	0.33	-0.4%	0.330	0.334	-1.2%	0.337	0.342	-1.5%
	2	0.32	0.32	0.0%	0.318	0.314	1.3%	0.322	0.326	-1.1%
Water	1	0.29	0.29	0.6%	0.273	0.276	-1.3%	0.263	0.275	-4.1%
	2	0.25	0.25	-0.9%	0.262	0.264	-0.8%	0.256	0.267	-4.3%
PTFE	1	0.51	0.52	-1.4%	0.511	0.519	-1.5%	0.523	0.520	0.6%
	2	0.48	0.48	-0.5%	0.479	0.483	-0.7%	0.486	0.481	0.9%
Magnesium	0.5	0.69	0.70	-1.6%	0.691	0.707	-2.2%	0.721	0.717	0.6%
Silicon	0.5	1.08	1.03	5.4%	1.08	1.03	5.4%	1.12	1.06	5.3%
	1	0.92	0.88	5.3%	0.923	0.876	5.4%	0.941	0.903	4.2%
Titanium	0.5	2.99	3.01	-0.5%	2.987	2.940	1.6%	3.021	3.014	0.2%
			Min.	-1.7%		**Min.**	-2.3%		**Min.**	-4.3%
			Max.	5.4%		**Max.**	5.4%		**Max.**	5.3%
			Mean |ε|	1.4%		**Mean |ε|**	1.8%		**Mean |ε|**	2.0%

Table 6. *Comparison of values for individual projections reported in this work to previous similar work at 160kV.*

		160kV Central Ray (DR) Results								
		Chen *et al.*			Lennox *et al.*			This Paper		
Material	Nominal Diameter (in.)	μ_{HADES} (cm^{-1})	μ_{Proj} (cm^{-1})	ε	μ_{HADES} (cm^{-1})	μ_{Proj} (cm^{-1})	ε	μ_{HADES} (cm^{-1})	μ_{Proj} (cm^{-1})	ε
Graphite	0.5	0.28	0.28	1.4%	0.284	0.284	0.0%	0.280	0.284	-1.4%
	1	0.26	0.25	2.4%	0.260	0.252	3.2%	0.257	0.257	-0.1%
	2	0.27	0.27	1.4%	0.271	0.267	1.5%	0.269	0.270	-0.2%
Acetyl Copolymer	0.5	0.24	0.24	0.7%	0.237	0.237	0.0%	0.236	0.241	-1.8%
	1	0.24	0.24	0.5%	0.239	0.235	1.7%	0.237	0.240	-1.4%
	2	0.24	0.23	1.2%	0.236	0.232	1.7%	0.235	0.236	-0.6%
Water	1	0.20	0.20	1.5%	0.192	0.188	2.0%	0.177	0.188	-6.1%
	2	0.18	0.17	1.3%	0.187	0.184	1.1%	0.177	0.187	-5.4%
PTFE	1	0.34	0.33	1.3%	0.339	0.335	1.2%	0.337	0.338	-0.5%
	2	0.34	0.33	3.1%	0.340	0.329	3.3%	0.338	0.335	1.1%
Magnesium	0.5	0.33	0.32	2.0%	0.326	0.326	0.0%	0.324	0.328	-1.4%
Silicon	0.5	0.49	0.46	7.2%	0.491	0.459	6.9%	0.485	0.466	4.1%
	1	0.48	0.46	5.1%	0.485	0.462	5.1%	0.478	0.465	2.8%
Titanium	0.5	1.41	1.34	5.6%	1.412	1.334	5.8%	1.383	1.361	1.6%
			Min.	0.5%		**Min.**	0.0%		**Min.**	-6.1%
			Max.	7.2%		**Max.**	6.9%		**Max.**	4.1%
			Mean |ε|	2.5%		**Mean |ε|**	2.4%		**Mean |ε|**	2.0%

Table 7. *Comparison of this work with previous HADES estimated CT values using the "full-radiograph" Single-Ray-Path Method (this work) and the single-pixel-radiograph (slab) method (Lennox et al.). Experimental values above have been corrected for systematic changes in the detector response by using Eqs(1a) and (1b).*

		100kV					160kV				
		CT EXPT.	***HADES Mean Attenuation*** Lennox *et al.* [Lennox 2014]		***HADES Mean Attenuation*** This work		***CT EXPT.***	***HADES Mean Attenuation*** Lennox *et al.* [Lennox 2014]		***HADES Mean Attenuation*** This work	
Material	Nominal Dia. (in.)	μ_{CT} (cm^{-1})	μ_{HADES} (cm^{-1})	ε	μ_{HADES} (cm^{-1})	ε	μ_{CT} (cm^{-1})	μ_{HADES} (cm^{-1})	ε	μ_{HADES} (cm^{-1})	ε
Graphite	0.5	0.343	0.330	-3.9%	0.333	-3.0%	0.278	0.285	2.5%	0.280	0.7%
	1	0.325	0.318	-2.1%	0.322	-1.1%	0.251	0.260	3.4%	0.257	2.3%
	2	0.401	0.377	-5.9%	0.381	-4.9%	0.265	0.272	2.4%	0.269	1.5%
Acetyl Copolymer	0.5	0.317	0.300	-5.2%	0.305	-3.8%	0.234	0.240	2.5%	0.236	0.7%
	1	0.332	0.316	-4.7%	0.322	-2.9%	0.234	0.239	2.1%	0.237	1.0%
	2	0.363	0.344	-5.2%	0.351	-3.2%	0.232	0.237	2.0%	0.235	1.2%
Water	1	0.251	0.240	-4.3%	0.247	-1.6%	0.175	0.178	1.9%	0.176	0.9%
	2	0.269	0.257	-4.3%	0.261	-2.8%	0.174	0.178	2.3%	0.177	1.6%
PTFE	1	0.560	0.534	-4.6%	0.550	-1.8%	0.333	0.341	2.4%	0.336	1.2%
	2	0.635	0.599	-5.7%	0.623	-1.9%	0.329	0.342	4.1%	0.339	3.2%
Mg	0.5	0.699	0.694	-0.7%	0.725	3.7%	0.319	0.330	3.4%	0.323	1.4%
Si	0.5	1.116	1.200	7.6%	1.250	11.8%	0.457	0.500	8.7%	0.490	6.3%
	1	1.119	1.182	5.6%	1.212	8.3%	0.456	0.489	7.1%	0.481	5.4%
Ti	0.5	4.799	5.138	7.1%	4.871	1.5%	1.308	1.483	13.4%	1.429	9.3%
			Min.	-5.9%	**Min.**	-4.9%		**Min.**	1.9%	**Min.**	0.7%
			Max.	7.6%	**Max.**	11.8%		**Max.**	13.4%	**Max.**	9.3%
			Mean|ε|	4.8%	**Mean|ε|**	3.7%		**Mean|ε|**	4.2%	**Mean|ε|**	2.6%

8. Summary

The chief objective of this work has been to investigate the impact of recent changes in HADES modeling and experiment analyses upon validation results. The primary change in HADES has been revising the spectral model of the HEAF MicroCT. Aufderheide [Aufderheide, 2014] has recalculated the baseline spectral response of the Thales Flashscan 33 panel detector and the spectral intensity of the Yxlon D-09 450kV x-ray tube. To remove statistical bias from the distribution of modeling errors, we have inserted an *ad hoc* 1.6359mm-thick aluminum filter in the simulated x-ray beam. The main change in analysis of experimental data has been to compensate for a drop-off of system response that occurred over the five months in which measurements were taken. The specimens are fourteen homogeneous right circular cylinders of various materials, ranging between ½ and 2 inches in diameter. Each is chemically well characterized and of a known, uniform density. The measured LACs come from reconstructed images of computerized tomographic (CT) x-ray scans and from analyses of individual digital radiographs (DR) obtained during those scans. Each specimen is scanned only once at 160kV and once at 100kV.

We find the changes above have no obvious effect on the overall accuracy of the model. Table 8 summarizes the spread of modeling errors and compares this work to previous works by Chen *et al.* and Lennox *et al.* [Chen, 2011, Lennox 2014(1) and 2014(2)]

Table 8. *Summary* **c***omparison of modeling errors* ε *between HADES simulations and measurements for a set of 14 specimens scanned with the HEAF MicroCT system in 2010.*

Type of Data	Max Photon Energy	Reference	Error, ε		
			Min ε	Max ε	Mean$\lvert\varepsilon\rvert$
Central-ray LAC from DR Images (Beam hardening uncompensated)	100 kVp	This work	-4.3%	5.3%	2.0%
		[Chen 2011]	-1.7%	5.4%	1.4%
		[Lennox 2014(1)]	-2.3%	5.4%	1.8%
	160 kVp	This work	-6.1%	4.1%	2.0%
		[Chen 2011]	0.5%	7.2%	2.5%
		[Lennox 2014(1)]	0.0%	6.9%	2.4%
Mean LAC from CT Images (Beam hardening compensated for μ_L)	100 kVp	This work	-4.9%	11.8%	3.7%
		[Lennox 2014(2)]	-5.9%	7.6%	4.8%
	160 kVp	This work	0.7%	9.3%	2.6%
		[Lennox 2014(2)]	1.9%	13.4%	4.2%

The magnitudes of the modeling errors are such that their means over the set of all materials studied are smaller than 5% and are about three times less than their maximum values. By *modeling error* we mean the difference between the model and the measurement relative to the measured value, Eq(7). The results in this work are similar to previous HADES validation efforts to date, all of which use the same experimental data as we [Chen 2011, Lennox 2014(1) and 2014(2), Aufderheide 2013]. Although the ranges of modeling errors are similar, the distribution of errors among the specimens varies somewhat from report to report, due to minor changes in the analyses of the experimental data and small changes in the HADES spectral model. We find, as Lennox *et al.* did previously [Lennox 2014(1) and 2014(2)], that the modeling errors using DR-derived LAC values are about half the magnitude of the modeling errors using CT-derived LAC values. Note that the errors may be due to modeling, measurements or both. It is desirable to minimize the errors, but this is a goal for future work.

9. Future work

The following opportunities for future work exist:

- Improve the experimental accuracy and stability of the microCT measurements.
- Repeat each microCT scan at least 2 times to improve statistical confidence.
- Compare HADES to experiment in units of LMHU.
- Collate existing HADES estimates from all of the single-specimen summary statistics reports and check the error range for mean LAC values over a large variety of materials. (The errors are almost certainly going to be much larger for the inhomogeneous materials in those reports than they were for the well characterized, homogeneous, uniforμλy dense materials in this study.)
- Simulate full CT scans and reconstructions, comparing simulations to experimental CT scans.

- Determine the amount of error involved in the single-ray approximations to CT measurements. (Are full CT simulations intrinsically more accurate numerically than the single-ray "mean LAC" approximation?)
- Extend the microCT validation to other materials and possibly other voltages.
- Do a detailed comparison of HADES to measurements on the upgraded HEAF MicroCT System.
- Develop and test HADES models for other systems, including commercial systems.

10. References

[Aufderheide 2000] M. B. Aufderheide, D. M. Slone, A. E. Schach von Wittenau, "HADES, A Radiographic Simulation Code," *Review of Progress in Quantitative Nondestructive Evaluation, vol. 20A,* AIP Conf. Proc. 557, pp. 507-513 (2000).

[Aufderheide 2004] M. B. Aufderheide, G. Henderson, A. E. Schach von Wittenau, D. M. Slone, H. E. Martz, "HADES, a code for simulating a variety of radiographic techniques," 2004 IEEE Nuclear Science Symposium Conference Record, Volume 4, pp. 2579 – 2583, Digital Object Identifier 10.1109/NSSMIC.2004.1462780 (2004).

[Aufderheide 2007] M. B. Aufderheide, private communication.

[Aufderheide 2013] M. B. Aufderheide, S. G. Azevedo, W. D. Brown, K. M. Champley, J. S. Kallman, H. E. Martz, K. E. Morales, I. M. Seetho, J. A. Smith, E. O. Updike, and W. T. White III, Validation of the HADES Radiographic Code for Two Low Energy Radiographic Systems, LLNL-TR-0616601 (Dec 19, 2013).

[Bond 2013] K. P. Bond and D. Schneberk, IMGREC Manual, LLNL-SM-616032, (Feb. 5, 2013).

[Briesmeister 2000] J. F. Briesmeister, "MCNP--A general Monte Carlo n-particle transport code," Technical Report LA-13709-M, Los Alamos National Laboratory (2000).

[Butler 2002] L. E. Butler and E. W. Edwards, "BRL-CAD Tutorial Series: Volume I – Overview and Installation", ARL-SR-113, February (2002). (Also see BRL-CAD website, brlcad.org.)

[Chen 2011] H. Chen, M. B. Aufderheide III, W. T. White III, G. P. Roberson and L. G. Glascoe, "Validation of HADES-based Simulations of Radiographic Experiments at LLNL," presented at the IEEE International Conference on Technologies for Homeland Security, Waltham, MA, United States, November 15, 2011 through November 17, 2011, LLNL-PROC-489645, (June 23, 2011).

[Cullen 1989] D. E. Cullen, M. H. Chen, J. H. Hubbell, S. T. Perkins, E. F. Plechaty, J. A. Rathkopf, and J. H. Scofield, "Tables and Graphs of Photon-Interaction Cross

Sections from 10 eV to 100 GeV Derived from the LLNL Evaluated Photon Data Library (EPDL), Parts A and B, UCRL-50400, Vol. 6A and 6B, Rev 4 (1989).

[de Jonge 2004] M. D. de Jonge, C. Q. Tran, C. T. Chantler, Z. Barnea, "Improved techniques for measuring x-ray mass attenuation coefficients," in Proc. of SPIE Vol. 5538, *Optical Constants of Materials for UV to X-Ray Wavelengths*, R. Soufli and J. F. Seely (eds.), SPIE, Bellingham, WA (2004, pp 96–106.

[deMicco 2012] M. F. deMicco and W. T. White III, "MicroCT: Reconstructing X-ray Computerized Tomographic Images from Data Acquired on LLNL MicroCT Systems," IDD-MCT-SOP-004, (2012).

[Kallman 2012] Jeffrey S. Kallman, Isaac M. Seetho, Harry E. Martz, Jr., William D. Brown, "Differences Between MicroCT Automated Analysis Versions 1.2.1 and 1.3," LLNL-TR-555651 Version #1, (April 17, 2012).

[Krauss, 2009] R. Krauss, "Industrial Computed Tomography System Data Collection of Home-Made Explosives," B-09-11-S-v_08, DHS/STD/TSL-XX-XX, (2009) [Limited Distribution].

[Lennox 2011] K. P. Lennox, H. Chen, M. B. Aufderheide, W. T. White III, G. P. Roberson, J. Smith, L. G. Glascoe, "Validation of HADES MicroCT Radiograph Prediction," Abstract of talk presented at the 2011 DoE Conference on Data Analysis, held in Santa Fe, NM, March 1, 2011 and March 2, 2011, LLNL-ABS-519872 (Dec. 9, 2011).

[Lennox 2012] K.P. Lennox, W. T. White III and L. G. Glascoe, "A Variability Study of MicroCT Reference Samples," LLNL-TR-572912 (2012).

[Lennox 2014(1)] K.P. Lennox, M. B. Aufderheide, W. T. White III, G. P. Roberson, J. A. Smith and L. G. Glascoe, "Validation of HADES Predictions for Full Radiographs," LLNL-TR-639523 (2014).

[Lennox 2014(2)] K. P. Lennox, M. B. Aufderheide, W. T. White III, G. P. Roberson, J. A. Smith, and L. G. Glascoe, "HADES Single-Ray Model Validation", LLNL-TR-651696 (2014).

[Lennox 2014(3)] K. P. Lennox, private correspondence, "muCT correction rules," e-mail to K. P. C. Bond, (Jan., 10, 2014).

[Maienschein 2012] J. Maienschein, "A Home for Energetic Materials and Their Experts," *Energy and Technology Review*, UCRL-TR-52000-12-7/8 (July 9, 2012).

[Schneberk 2009] D. J. Schneberk, W. D. Brown, H. E. Martz Jr., "IMGREC 2.8.5.7c16 – Compatibility with older versions, new commands and features," LLNL-TR-XXXXX-DRAFT, (June 2, 2009) [LLNL internal document].

[Schneberk 2010] D. Schneberk, "Appendix III — LLNL process for calculating Beam Hardening Corrections," in "CT Processing/Reconstruction for HEAF/Tyndall acquired data of Home Made Explosives Materials," Version 1.7, (March 25, 2010). [Internal LLNL note; File Name & date: Recon-SOP-HEAF-9slit.doc, 9/21/2010.]

[Seetho 2011] I. M. Seetho, W. D. Brown, J. S. Kallman, H. E. Martz Jr., W. T. White III, “MicroCT: Automated Analysis of CT Reconstructed Data of Home Made Explosive Materials Using the Matlab MicroCT Analysis GUI,” LLNL-TR-503291, (October 6, 2011).

[Smith 2011] J. A. Smith, D. J. Schneberk, J. S. Kallman, H. E. Martz Jr., D. Hoey, R. Krauss and R. Klueg, "Documentation of the LLNL, TAFB and TSL micro-CT systems," LLNL-TR-421377 Rev A, (Jan. 3, 2011).

[Smith, 2013], J. A. Smith, *Ze: an Effective Atomic Number for Polychromatic X-ray Transmission*, LLNL-JRNL-640273, (July 3, 2013).

[Watkins, 2013] “Radiographic Simulation Methods and Results,” *The Detonation, Safety, and Radiography Detection Properties of Potassium Chlorate/Fuel Explosives*, Vol. 2, B. E. Watkins, B. C. Tappan, and J. E. Parmeter, eds., LLNL-TR- 638946, Section 2.9 (2013) [Limited Distribution].

11. APPENDIX A — TP35 Reference Materials Excluded from Consideration in this Report

a. The TP35 experiments for one inch Magnesium and one inch Aluminum [Chen 2011] appear to be outliers. When the QA bounds for these experiments were investigated by Lennox *et al.* [Lennox 2012], they did not meet the tolerance bounds and are therefore omitted from the HADES validation.
b. Our HADES model does not model a bottle container. This contributes significantly to error in the HADES predictions for the ½ inch bottle of water (to a much larger extent than the one inch and two inch bottles of water). Therefore the half inch bottle of water referenced by Chen et al. [Chen 2011] will not be considered in these HADES Validation results.
c. In the experiment for half inch PTFE, the reference specimen on the bottom carousel of MCT-HEAF scanner, was missing. The data processing to determine the projection closest to the source (explained in detail in Appendix C) relies on all six reference specimens being present on the bottom shelf. Since the attenuation cannot be estimated from the raw projection data, the half inch PTFE is also not considered in the HADES Validation results.

12. APPENDIX B — Detailed Steps for Estimating μ from CT values

1. **Create attenuation radiographs that are compensated for fluctuations in x-ray intensity and beam hardening.** A background irradiance image (empty field of view between the collimator and the detector panel) and all 400 of the images in a scan are flat-fielded and linearized — *i.e.*, corrected pixel by pixel for spatial variations in offset and gain in the detector panel and then median filtered to remove bad pixels. Each of the 400 flat-fielded scan images is then divided pixel-wise by the flat-fielded background image. A small patch of unobstructed pixels (a "postage stamp" region) is monitored to account for changes in the source intensity, and 400 ratio images of I_o/I are created, where I denotes the measured irradiance transmitted by the test object and I_o denotes the background irradiance. The natural logarithm of each ratio image is then calculated, $\ln(I_o/I)$, creating an attenuation radiograph from each ratio image. Next, the attenuation radiographs are compensated for beam hardening by multiplying the value in each pixel by an empirically determined function, Eq (3) in the body of the report. At 160kV, the materials of interest to LEDP exhibit little or no beam hardening, and beam hardening is ignored. At 100kV, however, beam hardening can be pronounced, producing a scoop-shaped profile. Beam hardening compensation (BHC) in the TP35 images has been accomplished with a polynomial whose coefficients were determined from measurements of cylinders of an aluminum alloy. For materials with a mean atomic number near that of aluminum (13), the BHC function works well, but for materials of lighter elements (C, H, N, O), the BHC function overcorrects for the beam hardening.

2. **Create a CT reconstruction.** A fan-beam CT algorithm processes the attenuation radiographs to reconstruct a 3-D representation of the cylindrical test object. Each volume element (voxel) in the 3-D image holds a scalar value that represents the CT-estimated value of μ at that location in the test object.
3. **Get attenuation coefficient from Analysis output**: Using LEDP's standard procedure for analyzing reconstructed CT images [Seetho 2011], the 3D image is then segmented, eroded away from the boundary to minimize the effect of partial volume at the boundaries, and the mean attenuation coefficient of the remaining voxels is calculated .
4. **Correct for reconstruction code error**: Due a bug in the image reconstruction software that was used to reconstruct the raw data but which was fixed at some point during the TP35 time frame, some of the data contains a 10% error in attenuation. To correct for this, if the attenuation for the water reference specimen was below 0.0225 for 100Al channel and below 0.016 for 160Alcu channel then the attenuation coefficient is multiplied by (1/0.9).
5. **Correct for the drop-off in attenuation**: Eqs(1a) and (1b) in the body of the report are applied to compensate for system drift.

13. APPENDIX C — Finding the Angular Projection in which the Test Specimen is Closest to the Source and Centered on Axis

The procedure outlined below is adapted from [Lennox 2012].

1. **Determine the boundaries of the top and bottom slits in each DR.** An edge-detection algorithm is run on a DR projection to produce a binary edge map (1 for edge pixels and 0 for everything else). Then, starting from the top-most row in the image, the first row for which the sum of the pixels in the edge map is greater than a threshold is marked as the top of the top slit. Similarly, starting from middle row in the image, the first row above it for which the sum of the pixels in the edge map is greater than a threshold is marked as the bottom of the top slit.

   The process is repeated for the bottom slit. Starting from the middle row of the image, the first row below it for which the sum of the columns in the edge map is greater than a threshold is marked as the row number of the top of the bottom slit. Similarly, starting from last row in the image, the first row above it for which the sum of the columns in the edge map is greater than a threshold is marked as the bottom of the bottom slit.

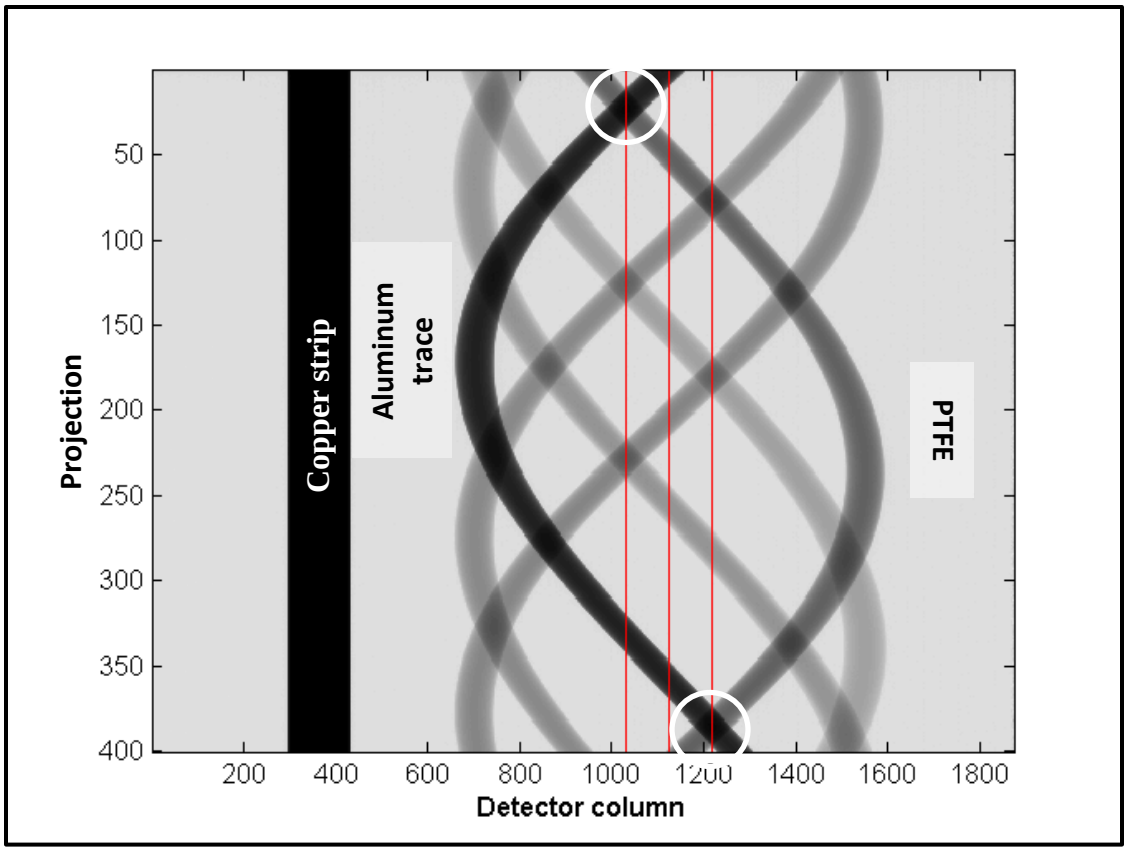

Figure C-1. *Sinogram of the bottom slit. The traces corresponding to the aluminum and PTFE are indicated, and their cross-over points are circled. The outer two red lines mark the columns where the PTFE and aluminum reference specimens cross. The center red line marks the column containing the projected center of rotation.*

2. **Make sinograms for the lower and upper slits.** Calculate the center row for each slit as the arithmetic mean of the slit's top and bottom row numbers. Generate a transmission radiograph by taking the column-wise median of the 5 central rows of the slit and normalizing it by I_o, the background irradiance image (a scan collected with each measurement with the slits but without the main or reference specimens present). Then generate a sinogram from all the projections collected in the measurement for the center of the bottom slit (Figure C-1). Repeat for the upper slit.
3. **Determine the column number of the projected center of rotation**: From the sinogram of the lower slit, locate the two instances when the PTFE reference specimen crosses the aluminum reference specimen, as illustrated by the white circles in Figure C-1. [Lennox 2013] This happens at the first and last projection with exactly 4 local minima (not considering the copper strip). Local minima are defined as points in a smoothed version of the sinogram, that are the minima of the 21 points surrounding points (10 on either side) and where the 21 surrounding points have a mean less than 0.95. Once the column numbers of the two crossing points of the PTFE and Aluminum references specimens are determined, the projected center of

rotation is found as the column midway between the two crossing points. In Figure C-1, the outer two red lines mark the cross-over points. The center red line marks the column that contains the projected center of rotation of the specimen.

4. **Determine the projection in which the specimen is closest to the source**: From the sinogram for the top slit, determine the projection in which the image of the specimen is symmetric about the projected center of rotation and is widest (for the case that the specimen crosses the center of rotation two times). Call this projection the centered projection of the specimen. Use the positions of the left and right edges of the specimen — calculated as the locations of the maximum and minimum of the finite difference of that projection along the slit — to find the centered projection of the specimen.

14. APPENDIX D — Description of HADES as used in the present work.

Figure D-1 depicts the use of HADES for simulating a measurement on the HEAF MicroCT System.

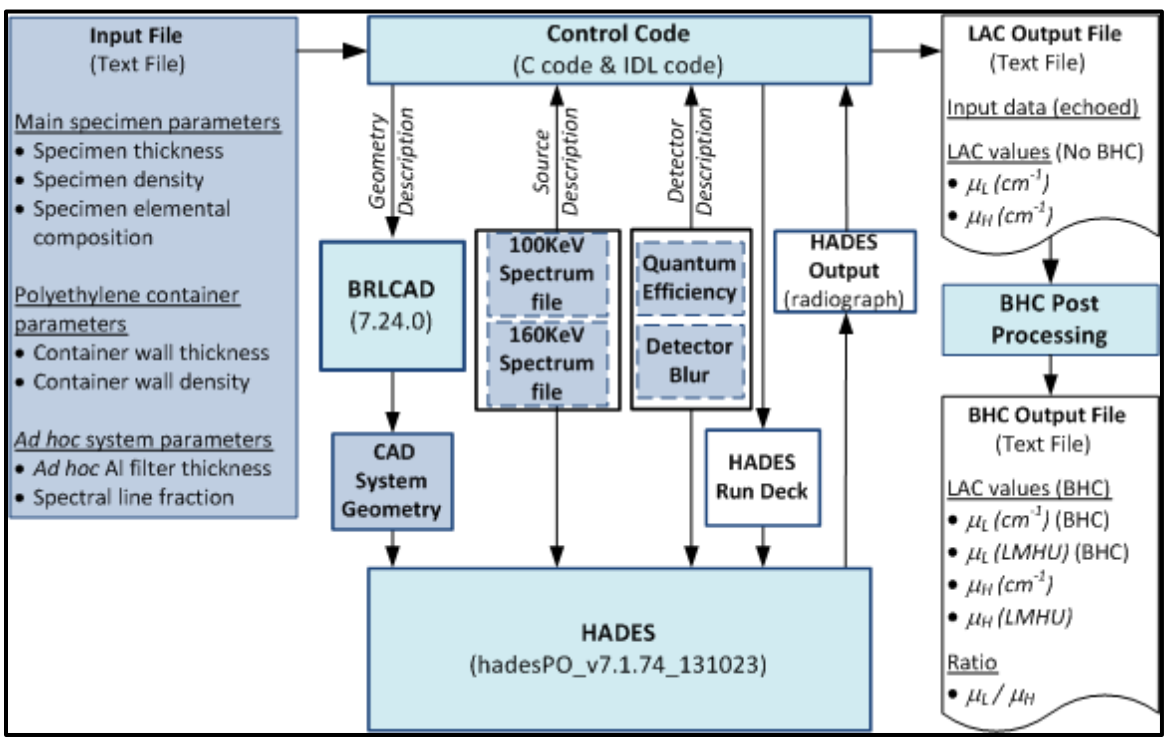

Figure D-1. *Data flow for simulating HEAF MicroCT measurements with HADES.*

As shown in the figure, HADES accepts an input text file that specifies the composition, density and diameter of the MicroCT specimen, the wall thickness and density of a container that holds the specimen, and optional values of parameters used to make small adjustments on the baseline source spectrum. The latter include the thickness of an *ad hoc* aluminum filter and a numerical factor that changes the relative strength of line and continuum emissions from the HEAF MicroCT x-ray tube. In this work, we use 1.6359

mm as the thickness of the *ad hoc* aluminum filter and a value of 1 for the spectral line factor. Section 6 of this report discusses how we derive those values. HADES assumes that the specimen of interest is held in a polyethylene container, but the user may choose to eliminate the container from a simulation. When a container is used, the input file specifies the wall thickness and mass density of the container.

A MicroCT-system-specific Control Code controls the overall action of HADES, including reading input, defining the properties of the radiographic system, and producing MicroCT-tailored output. The Control Code links to BRL-CAD [Butler 2002] to create a detailed geometric model of all components of the system and enable HADES to calculate ray paths easily. The Control Code also connects HADES to external data files that model the spectral properties of the x-ray source and define the blur and spectral response of the detector. It creates the HADES Run Deck, a set of command lines and parameter values that direct the HADES calculations for each radiograph. While the HADES Run Deck can be created manually, it is better constructed by the MicroCT-specific Control Code. Finally, the Control Code enables HADES to simulate time-varying system changes and to turn on or off various features of the HADES code. This feature permits simulating a full CT scan with one HADES run.

The modules included in Figure D-1 are:

<u>HADES.</u> The version of HADES used in this work is *hadesPO_v7.1.74_131023*.

<u>BRLCAD.</u> BRLCAD [Butler 2002] generates a CAD model of the MicroCT experimental setup using input from a control code. The version of BRLCAD used in this work is 7.24.0.

<u>Control Code.</u> The control code is a few C and IDL source files that control setup of the HADES model and then call the main HADES application to generate a MicroCT radiograph. It gets input from a text input file and a set of static data files and generates a text output file that is processed manually to apply experimentally derived BHC parameters to the calculated LAC values. Certain parts of the MicroCT system model are hard-coded into the Control Code, such as the composition, density, dimensions and placement of the MicroCT reference specimens and collimator. The version of the suite of control and x-ray system files used in this work is Version 1.5.

<u>Input Text File.</u>

- <u>Diameter, density, and chemical composition of the specimen being simulated</u>. These are arguments that the code expects at the command line. They currently must be specified in the input file.
- <u>Wall thickness and density of the specimen container</u>. A plastic vial or bottle holds the liquids and powders tested in the HEAF MicroCT. In this work the container is excluded from the model.
- <u>*Ad hoc* Aluminum filter</u>. The thickness of the *ad hoc* filter is an input argument that must be specified in the input file that the current version of the HADES code expects at the command line. As discussed in the body of this paper, selecting the thickness value of 1.6359 mm reduces the mean error to zero for 100Al.

- Spectral line fraction. This factor is available to adjust the ratio of power in the source line spectrum to power in the Bremsstrahlung continuum if desired. The default value of the factor in the baseline code is 1.0. Currently, this argument must be specified in the HADES input file. As mentioned in Section 6, adjusting this parameter does not seem to improve agreement between model and measurement for presently available data. We recommend leaving the parameter set to 1.0.

X-ray system Files.

- Two baseline source spectra. Spectra are 100kV with an aluminum filter (denoted "100Al") and 160kV with an aluminum filter plus a copper filter (denoted "160AlCu"). Each source spectrum is provided via a computer file that is part of the baseline HADES model code for the HEAF system. NOTE: the baseline spectral files used in the latest version of HADES differ slightly from those used in previous versions. Furthermore, previous validation tests by Chen *et al.* and Lennox *et al.* used the previous spectral files, which included no additional *ad hoc* filtering by aluminum.
- DQE (detector quantum efficiency) file. This file is by default part of the HADES Model code base, but the user may if desired provide a different DQE file. Currently the file represents the Thales Flashscan 33 panel detector used by the HEAF MicroCT system.
- Detector blur function (PSF). This file is by default part of the HADES Model code base, but the user may if desired provide a different blur function file. The current PSF is an energy-dependent model for the Thales Flashscan 33 detector.
- CAD model. The 3-D computer-aided design (CAD) model describes the collimators, specimens, specimen holder and other key parts of the system in terms of the shape, location, orientation and size. Currently the CAD model is built by BRLCAD, which is called automatically by the Control Code.

15. Appendix E — Mean LAC over a circular cylinder in a collimated, uniformly intense x-ray beam.

Consider a right circular cylinder of diameter D in a uniformly intense, collimated beam of x-rays with the direction of x-ray propagation being transverse to the axis of the cylinder, as in Figure E-1.

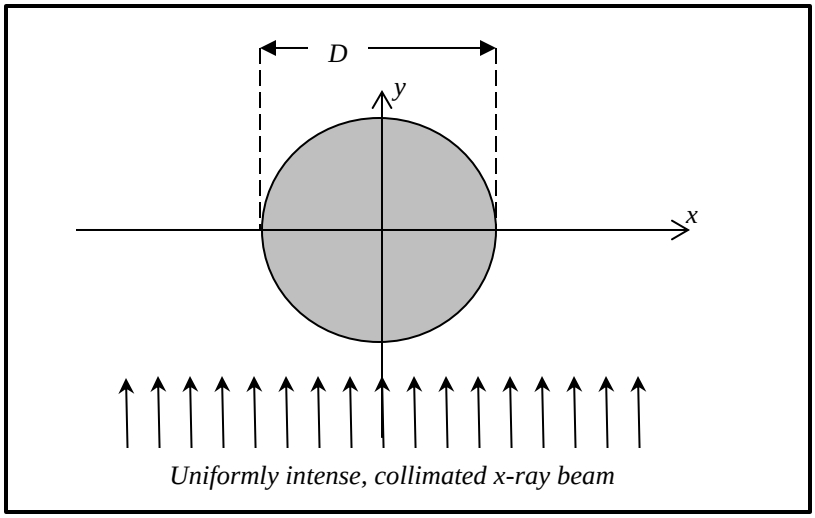

Figure E-1. *Circular cross section of a cylinder of diameter D in a uniformly intense, collimated x-ray beam.*

Suppose that $\mu(L)$, the LAC along a ray with path length L through the material, is

$$\mu(L) = \mu_o - \mu_1 L\,, \tag{E.1}$$

where $\mu_1 L$ is, to first order, the beam-hardening along the ray. The parameters μ_o and μ_1 depend upon spectral illumination and the composition and density of the material constituting the cylinder. They are independent of path length L. From Eq(E.1), the mean value of $\mu(L)$ over all rays, denoted $\overline{\mu}$, is

$$\overline{\mu} = \mu_o - \mu_1 \overline{L}, \tag{E.2}$$

where $\overline{L}$ is the mean path length across the circle. Combining Eqs(E.1) and (E.2), one has

$$\overline{\mu} = \mu\left(\overline{L}\right), \tag{E.3}$$

In other words, Eq(E.3) says that in a collimated x-ray beam when beam hardening is weak, the mean value of the beam hardened LAC of a cylinder is the LAC evaluated over the mean path length $\overline{L}$. For a circle,

$$\overline{L} = \frac{\pi D}{4}. \tag{E.4}$$

Thus,

$$\overline{\mu} = \frac{4}{\pi D} \ln\left(\frac{I_o}{I}\right)\Bigg|_{L=\pi D/4}, \tag{E.5}$$

where the subscript in Eq(E.5) means that I is calculated along a single ray of path length $L = \pi D/4$ through the cylinder.